HHS Public Access

Author manuscript

*Nano Lett*. Author manuscript; available in PMC 2019 April 15.

Published in final edited form as:

*Nano Lett*. 2018 September 12; 18(9): 5839–5845. doi:10.1021/acs.nanolett.8b02498.

# Graphene-dendrimer nanostars for targeted macrophage overexpression of metalloproteinase 9 and hepatic fibrosis precision therapy

**Pedro Melgar-Lesmes**[1,2,3], **Aureli Luquero**[2], **Marina Parra-Robert**[4], **Adriana Mora**[2], **Jordi Ribera**[4], **Elazer R. Edelman**[1,5], and **Wladimiro Jiménez**[2,4]

[1]Massachusetts Institute of Technology, Institute for Medical Engineering and Science, 77 Massachusetts Ave, Cambridge, MA 02139, USA.

[2]Department of Biomedicine, School of Medicine, University of Barcelona, 143 Casanova, 08036 Barcelona, Spain.

[3]Fundació Clínic per a la Recerca Biomèdica, Hospital Clínic Universitari, IDIBAPS, 149 Rosselló, 08036 Barcelona, Spain.

[4]Biochemistry and Molecular Genetics Service, Hospital Clínic Universitari, IDIBAPS, CIBERehd, 170 Villarroel, 08036 Barcelona, Spain.

[5]Cardiovascular Division, Brigham and Women's Hospital and Harvard Medical School, 75 Francis St, Boston, MA 02115, USA.

## Abstract

Fibrosis contributes to ~45% of all deaths in industrialized nations but no direct anti-fibrotic therapeutic interventions exist to date. Graphene-based nanomaterials exhibit excellent versatility in electronics, and emerging trends exploit their properties for biomedical applications, especially for drug and gene delivery. We designed constructs of graphene nanostars linked to PAMAM-G5 dendrimer for selective targeting and delivery of a plasmid expressing the collagenase metalloproteinase 9 under CD11b promoter into inflammatory macrophages in cirrhotic livers. Graphene nanostars preferentially accumulated in inflammatory macrophages M1 in less than three hours, in a manner unaffected by covalently linkage to dendrimers. Dendrimer-graphene nanostars efficiently delivered the plasmid encoding for metalloproteinase 9 into macrophages, allowing synthesis and secretion of the metalloproteinase to digest adjacent collagen fibers. In turn, metalloproteinase 9 overexpression promoted the macrophage switch from inflammatory M1

Corresponding Author: Pedro Melgar-Lesmes, PhD, -Massachusetts Institute of Technology, Cambridge, Massachusetts; 77 Massachusetts Avenue, Building E25-438. Cambridge, MA 02139. USA. Phone: +1 617-715-2026 FAX: +1 617-253-2514.; -Department of Biomedicine, School of Medicine, University of Barcelona, Casanova 143, 08036 Barcelona, Barcelona, Spain. Phone: +34 93-402-4524. FAX: +34 93-227-5697. pedroml@mit.edu; pmelgar@clinic.cat.

Author Contributions

P.M-L., A.L., M. P-R., A.M., and J.R. performed the experiments and analyzed the data. P.M-L., E.R.E. and W.J. designed the experiments and wrote the manuscript.

The Supporting Information is available free of charge on the ACS Publications website. Biological characterization of functionalized graphene nanostars, uptake kinetics of GNS, plasmid sequences, biodistribution of pSCR-DGNS in lung, spleen and kidney from cirrhotic animals, MMP-9 hepatic expression in mice treated with pMMP9-DGNS, liver weight in percentage, TIMP-1 and α-SMA expression in treated cirrhotic livers, and experimental procedures (Supporting Information PDF).

The authors declare no competing financial interest.

to pro-regenerative M2 in three days. This targeted gene therapy reduced selectively and locally the presence of collagen fibers in fibrotic tracts where inflammatory macrophages accumulated in cirrhotic mice without affecting the activation state of hepatic stellate cells. Overall this treatment significantly reduced hepatic injury and improved liver restoration in mice with liver cirrhosis treated for ten days.

Graphene-dendrimer nanostars targeted macrophage overexpression of metalloproteinase 9 selectively reducing hepatic fibrosis and might well treat diseases associated with fibrosis and inflammatory macrophages accumulation.

## Graphical Abstract

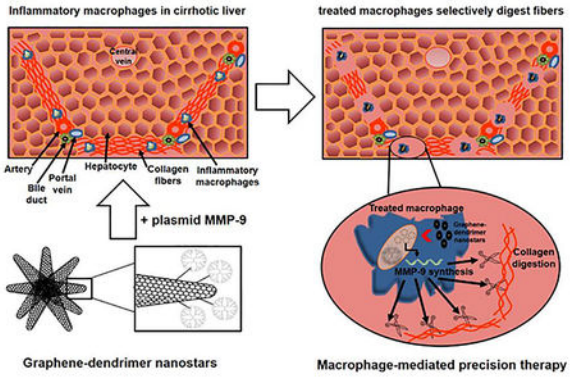


### Keywords

Graphene nanostars; dendrimer; fibrosis; macrophages; metalloproteinase; liver cirrhosis

Graphene nanostars (GNS) are clusters of conical rolls of graphene sheets with cone-shaped tips called nanohorns. Single-walled carbon graphene nanohorns are typically 2–5 nm in diameter and 40–50 nm in length. Thousands of graphene nanohorns form spherical aggregates (nanostars) of about 100 nm in diameter.[1] Their use has been increasingly applied to electronics, gas storage and energy applications.[2–6] However, research and development of GNS for biomedical applications is slowed by cluster formation that hinders functionalization of individual nanocones in biologically compatible solvents.[1] This limitation has been overcome with different approaches using organic solvents and high temperatures1 and the use of graphene nanohorns for therapy and diagnostics is rapidly emerging.[7–8] GNS, as most of nanoparticles, are mainly phagocytosed by macrophages and, in particular, by pro-inflammatory macrophages at diseased sites.[9] Actually carbon nanoparticles have been traditionally employed as a specific stain for macrophages skipping incorporation in dendritic cells.[10] GNS display an excellent biocompatibility, not inducing pro-inflammatory cytokines and degrading in few days.[11] Nanohorns that form GNS do not have the high aspect ratio issues related to toxicology already explored with carbon nanotubes[1] and do not require potentially toxic metal or chemical catalysts during synthesis such as occurs with other nanoparticles synthesis.[1] Moreover, the binding of GNS with PAMAM-G5 dendrimers can combine both macrophage selective targeting and nucleic acid cargo and delivery. This makes dendrimer-GNS (DGNS) a promising tool for a natural

targeting and treatment of macrophages present in areas with chronic inflammation where fibrosis occurs.

Fibrosis is the generic and common pathological endpoint to chronic injury. Fibrosis is the excessive accumulation of fibrous connective tissue (components of the extracellular matrix (ECM) such as collagen) in and around inflamed or damaged tissue, which can lead to lasting scarring, organ dysfunction and, ultimately, death.[12] Fibrosis contributes to nearly half of the deaths in developed countries.[13–14] Traditional treatments, including corticosteroids and immunosuppressants, have been fairly ineffective, with recent studies even suggesting that the their inhibition of macrophage activation interferes with control of fibrosis.[14] The fundamental challenge is that collagen synthesis is essential for tissue healing and remodeling - lethal when over-exuberant and harmful when suppressed. These processes and this delicate balance is most manifest in liver cirrhosis. Cirrhosis is one of the main causes of death and disability-adjusted life-years (DALY) worldwide.[15] Generally, cirrhosis develops after a long period of liver-cell injury that leads to the deposition of collagen, leading to progressive fibrosis and nodule formation in the liver tissue.[15] Different pharmacological[16–18] and nanotherapeutical[19] strategies have been developed over the years to act on different hepatic cell types to reduce liver fibrosis. Most of the efforts have been devoted to interfere with the transdifferentiation (or “activation”) of hepatic stellate cells (HSC) as they are the major cellular source of matrix protein-secreting myofibroblasts, and the major driver of liver fibrogenesis.[20–21] However the remarkable complexity and plasticity of HSC activation and regulation together with their interplay with other hepatic cell types limits specific removal of hepatic collagen without affecting inflammatory and healing processes.

Macrophages are abundant during all stages of tissue injury and repair and have an important influence on the progress and resolution of tissue damage.[22] After injury, resident tissue macrophages attract blood monocytes, which then differentiate into macrophages, and secrete an array of pro-angiogenic[23] and pro-inflammatory cytokines for activating HSC production of collagen to isolate tissue damage and avoid propagation.[13] Macrophages also play a pivotal role in ECM turnover and fibrosis regression, in part through expression of matrix metalloproteinases (MMP) especially MMP-9[24] and tissue inhibitors of metalloproteinases (TIMP).[25–26] However, when liver injury persists, activated HSCs and HSC-derived myofibroblasts continue to produce both collagen and TIMP-1, suppressing MMP-dependent degradation of collagen and inhibiting HSC apoptosis[27] Increased fibrogenesis and reduced fibrolysis results in excessive accumulation of ECM (i.e., pathological fibrosis) in hepatic tissue with a consequent loss of function. We sought to functionalize GNS for targeted overexpression of MMP-9 to determine if they could be preferentially taken up by inflammatory macrophages in liver fibrotic tracts in a controlled fashion that could then boost natural mechanisms of fibrosis regression.

## RESULTS AND DISCUSSION

Carbon nanoparticles have been traditionally employed to selectively stain macrophages.[28–29] We designed a method to functionalize commercially available carboxylated carbon graphene nanohorns using DMSO and to finally resuspend in a biologically compatible

solvent (Phosphate-Buffered Saline, PBS) with a clear focus for ***in vivo*** therapeutics. Free access of the crosslinking agents 1-Ethyl-3-(3-dimethylaminopropyl)-carbodiimide (EDC) / N-Hydroxysuccinimide (NHS) and generation 5 PAMAM dendrimer into GNS was facilitated by means of continuous ultrasonic agitation under constant temperature at 25 °C for 2 hours. We obtained GNS composed of graphene nanohorns coated with dendrimer (Figure 1A). Transmission Electron Microscopy (TEM) images revealed carboxylated GNS of 93.1 ± 1.5 nm (Figure 1B) that rose to 107.2 ± 1.5 nm when PAMAM dendrimer was covalently incorporated (Figure 1C). GNS diameter visualized by TEM was twice smaller than the size of nanoparticles dispersed in PBS and measured by Dynamic Light Scattering (DLS). Hydrodynamic diameter of carboxylated GNS resulted in a Z-average size of 193.2 nm, denoting a highly hydrated corona and a high aggregation of GNS in PBS (Figure 1D). GNS also showed a negative zeta potential (−35.7 mV) due to the carboxylic groups and biologically interesting isotonic properties (Figure 1D). Z-average diameter of DGNS increased to 237.9 nm and zeta potential switched to positive (36.6 mV) resulting in hypertonic nanoparticle dispersions (Figure 1E).

Despite extensive applicability in the pharmaceutical field, the use of dendrimers in biological systems is constrained by inherent toxicity attributed to the interaction of surface cationic charge of dendrimers with negatively charged biological membranes promoting hemolytic, cellular and hematological toxicity.[30–31] Positively charged and hypertonic dispersions of DGNS cannot be used directly for intravenous administration but we wondered whether the addition of nucleic acids (negatively charged) in the form of a plasmid could improve the biocompatibility of DGNS while transforming these nanoparticles with inherent affinity for macrophages into a vehicle for gene therapy. The incubation of a plasmid DNA (pDNA) with DGNS promoted the switch from positive to negative zeta potential −27.37 mV, and the osmolality changed from hypertonic to isotonic (289±3 mOsmol/Kg).

Isotonic dispersion of pDNA-DGNS was tested for biocompatibility in human endothelial cells as the primary cell barrier in blood vessels and consequently the first biological point of contact with an intravenously administered formulation. Our results showed no harmful effects on human umbilical vein endothelial cells over 24 h using nanoparticle concentrations ranging from 5 to 500 μg/mL (Figure S1A).

The uptake of most of nanoparticles over 200 nm administered ***in vivo*** is conceptually assumed to involve mainly macrophages and, in particular, pro-inflammatory macrophages at diseased sites.[9, 32] We wondered whether both isotonic GNS and pDNA-DGNS would be selectively incorporated by inflammation-activated macrophages. First, we incubated murine macrophages RAW 264.7 with GNS in the presence or absence of TNF-α. The incorporation of GNS by inflamed or non-inflamed macrophages increased in parallel over time up to 60 minutes and then GNS uptake only continuously rose in the presence of TNF-α, reaching most of cells after 180 minutes (Figure S2). Then we incubated pDNA-DGNS with macrophages in the presence or absence of TNF-α, and observed identical fostered incorporation of nanoparticles by inflamed macrophages (Figure S1B). Afterwards we decorated DGNS with FITC to examine the intracellular fate of dendrimers after internalization in inflamed macrophages. After 24 h of incubation, FITC-DGNS were

internalized and degraded by macrophage enzymes, shifting the molecules of GNS to the periphery of the cells and dendrimer-FITC all over in the cell, including the cell nucleus (Figure S1C). These results suggested that these nanoparticles could be selectively incorporated by pro-inflammatory macrophages present in chronically inflamed livers where they could deliver pDNA-dendrimer into cell nucleus for an effective gene therapy.

The advantage of delivering nucleic acids using dendrimers has been widely described.[33] Dendrimers can escape from lysosomes by the proton sponge effect, opening pores in the nuclear membrane for pDNA or siRNA gene therapy.[34–35] We performed functional ***in vitro*** studies to analyze the gene therapy effectivity of pDNA-DGNS using two plasmids: a plasmid encoding for MMP-9 under a CD11b promoter and co-expressing enhanced GFP (eGFP) under the potent CMV promoter; and a control plasmid with a MMP-9 scramble sequence only expressing eGFP (Figure S3). In line with the outcomes of GNS uptake, pMMP9-DGNS were mainly phagocytized by macrophages stimulated with TNF-α, highlighted by the presence of high levels of intracellular eGFP in most of cells due to a strong plasmid transcription efficiency after 3 days of incubation (Figure 2A). Interestingly, pMMP9-DGNS incubated with macrophages and induced with TNF-α (CD11b promoter activator) demonstrated a clear switching effect in the macrophage phenotype, exemplified by a very high presence of mannose receptor (a M2-like phenotype marker) (Figure 2B).

This effect was associated with an increased expression of MMP-9 in inflamed macrophages treated with pMMP9-DGNS for 3 days (Figure 2C) as it is known that MMP-9 downregulates other genes related to M1-like inflammatory phenotype.[36–37] Therefore overexpressing MMP-9 with pMMP9-DGNS in inflamed macrophages promotes a profound biological change in the functionality of these cells. We then tested the capacity of macrophages treated with pMMP9-DGNS to digest collagen (FITC-gelatin), not only as a function of MMP-9 overexpression but also as a sign of this phenotypical transformation to M2 macrophages. RAW 264.7 macrophages seeded on FITC-gelatin coated plates and treated with pMMP9-DGNS for 5 days displayed a black halo as a consequence of the digestion of collagen and a green nuclear staining as a consequence of the eGFP expression (Figure 2D). A time-course quantitative analysis of FITC released to the medium (gelatinase activity assay) revealed that an exponential increase of collagen degradation due to pMMP9-DGNS started after 3 days of incubation only when TNF-α was present (Figure 2E). The degradation of collagen was much lower with or without pMMP9-DGNS in the absence of inflammatory stimulus (Figure 2E). This functional experiment was the rationale to select the schedule of administration in 3 days for ***in vivo*** experiments using an animal model with liver fibrosis.

Liver cirrhosis was induced in Balb/c mice with $CCl_4$ i.p. injections twice a week for 8 weeks. It is well-established that cirrhosis induction using this toxic promotes the formation of hepatic regenerative nodules surrounded by fibrotic tracts composed by dense collagen bundles and pro-inflammatory CD68-positive infiltrated macrophages.[18] Following the schedule of administration that we established in the ***in vitro*** studies, we intravenously administered pMMP9-DGNS or pScramble(pSCR)-DGNS every 3 days for 10 days to cirrhotic mice. We wondered whether pDNA-DGNS could be incorporated into liver inflammatory macrophages to efficiently act as gene therapy as occurred in the ***in vitro***

studies. To answer this question we visualized hepatic eGFP positive cells in cirrhotic mice treated with pSCR-DGNS and found high intracellular levels of eGFP specifically in inflammatory macrophages corresponding to those stained for the Ly6c (M1 surface marker) (Figure 3A) and those devoid of mannose receptor all along the fibrotic tracts in cirrhotic livers (Figure 3B). The presence of functional pSCR-DGNS was negligible in other organs such as lung and kidney, and very low in spleen from cirrhotic animals denoting the high selectivity of these nanoparticles for inflammatory macrophages in injured livers (Figure S4).

When cirrhotic animals were treated with pMMP9-DGNS we found a significant increase in the hepatic gene expression of MMP-9 (Figure S5) confirming the effectiveness of this gene therapy *in vivo*. We observed a heightened presence of macrophages expressing both eGFP and mannose receptor in fibrotic tracts, and few adjacent macrophages only displaying mannose receptor (Figure 3C). These outcomes do not mean that this therapy displays low efficiency. Quite the opposite, macrophages incorporating pMMP9-DGNS switch to M2 phenotype, release M2-cytokines such as IL-4 and IL-10, and these cytokines paracrinally promote the transformation of newly incorporated macrophages in fibrotic tracts during the next days after nanoparticles administration. Therefore, this treatment boosts a domino effect in nearby non-treated macrophages expanding the therapeutic effect of pMMP9-DGNS. Indeed, we found a quantitatively significant increase in the gene expression of M2 markers in cirrhotic livers of mice treated with pMMP9-DGNS (Figure 4A), and a significant decrease in two of the three analyzed M1 markers COX-2 and IL-1β (Figure 4B), denoting that this therapy collaterally switched pro-inflammatory M1 to M2-like pro-regenerative macrophages in cirrhotic livers. Macrophages displaying a M2 phenotype are actively involved in fibrosis regression and tissue regeneration.[38] Our results show that pMMP9-DGNS promoted an increase in liver size compared to animals receiving pSCR-DGNS (Figure S6) likely as a consequence of boosting vascular and tissue remodeling.[36]

To analyze whether the treatment with pMMP9-DGNS could selectively promote tissue remodeling in fibrosis, we stained collagen fibers with Sirius Red in livers from cirrhotic mice treated with pMMP9-DGNS or pSCR-DGNS. The selective overexpression of MMP-9 by pMMP9-DGNS in inflammatory macrophages of cirrhotic mice promoted a significant reduction in the presence and density of fibrotic tracts stained with Sirius Red (Figure 5A). In fact, this selective therapy with the collagenase MMP-9 reduced a 25% the collagen protein accumulation in cirrhotic animals (Figure 5B) without altering hepatic collagen gene expression (Figure 5C). This beneficial anti-fibrotic effect was translated to a significant reduction of hepatocyte damage (reflected by levels of serum-detectable transaminases) (Figure 5D) and therefore an improved liver function without affecting the synthesis of albumin or proteins (Figure 5E).

A non-selective overexpression of MMP-9 using intravenously injected adenovirus has already been described to reduce hepatic fibrogenesis but that effect could be masked by the absence of cell selectivity and the reaction of the immune system in the presence of a virus.[39] Actually the non-selective overexpression of MMP-9 promoted HSC inhibition and apoptosis by blocking TIMP-1 and α-smooth muscle actin (α-SMA) expression and that was the main cause for collagen reduction in fibrotic livers.[39] In contrast, we selectively

overexpressed MMP-9 in inflammatory macrophages inside of fibrotic tracts promoting a local degradation of collagen fibers instead of blocking collagen production in HSC. Indeed pMMP9-DGN do not affect HSC markers TIMP-1 and (α-SMA) in cirrhotic livers (Figure S7). These results confirm that our therapy is selective for degrading and reducing collagen fibers in fibrotic livers and specifically in fibrotic tracts where chronic inflammation and infiltration of macrophages occurs.

In conclusion, functionalized GNS can indeed deliver a plasmid encoding for the collagenase MMP-9 to inflammatory macrophages located in fibrotic tracts of cirrhotic livers without need for any additional modification or molecular targeting. Effect was substantiated in ***vitro*** and ***in vivo*** through heightened collagen degradation. Such cell-selective gene therapy also promoted a phenotypic switch in pro-inflammatory macrophages from M1 to M2-like pro-regenerative and anti-inflammatory macrophages, raising the intriguing idea that control of fibrosis requires or is at least correlated with change in macrophage phenotype. Such a paradigm links chronic fibrosis and persistent inflammation offering as well as means of affecting the former by interfering with or transforming the latter-boosting fibrosis resolution and wound healing without additional collateral damage to hepatocytes. Standard anti-inflammatory and anti-fibrotic drugs employed in chronic liver disease are eventually metabolized by dysfunctional hepatocytes promoting additional hepatic damage. In contrast, pMMP9-DGNS gene therapy promoted improvement of hepatic function and fibrosis regression in experimental cirrhosis by displacing the balance between ECM production and degradation with precision where the scar occurs. HSC activation and the healing processes were maintained with intact ECM formation in the rest of the liver. Selectively reducing the extension of collagen bundles that hampers hepatocyte proliferation allowed a higher regeneration of the injured organ.

This spatially and locally controlled cell therapy might be extended well beyond control of liver cirrhosis and through balanced and precision maintenance of ECM to the full range of diseases associated with fibrosis and inflammatory macrophages accumulation.

## Supplementary Material

Refer to Web version on PubMed Central for supplementary material.

## Acknowledgments

Funding Sources

This work was supported by a grant from Ministerio de Economia y Competitividad (SAF2015–64126-R) to W.J.; from National Institutes of Health (R01 GM 49039) to E.R.E; from European Association for the Study of Liver (EASL), Generalitat de Catalunya (PERIS SLT002/16/00341) and AGAUR Beatriu de Pinos Program 2016 (BP-00236) to P.M-L.

## ABBREVIATIONS

| | |
|---|---|
| **ECM** | Extracellular Matrix |
| **MMP** | metalloproteinases |

| | |
|---|---|
| **TIMP** | tissue inhibitors of metalloproteinases |
| **TNF-α** | tumor necrosis factor alpha |

## REFERENCES


1. Karousis N; Suarez-Martinez I; Ewels CP; Tagmatarchis N, Chem Rev 2016, 116 (8), 4850–83. [PubMed: 27074223]
2. Izadi-Najafabadi A; Yamada T; Futaba DN; Yudasaka M; Takagi H; Hatori H; Iijima S; Hata K, ACS Nano 2011, 5 (2), 811–9. [PubMed: 21210712]
3. Song HS; Kwon OS; Kim JH; Conde J; Artzi N, Biosens Bioelectron 2017, 89 (Pt 1), 187–200. [PubMed: 27020065]
4. Murata K; Hashimoto A; Yudasaka M; Kasuya D; Iijima S, Adv. Mater 2004, 16 (17), 1520–1522.
5. Gatica SM; Nekhai A; Scrivener A, Molecules 2016, 21 (5).
6. Ohba T, ACS Nano 2014, 8 (11), 11313–9. [PubMed: 25347389]
7. Yang J; Su H; Sun W; Cai J; Liu S; Chai Y; Zhang C, Theranostics 2018, 8 (7), 1966–1984. [PubMed: 29556368]
8. Zhao H; Ding R; Zhao X; Li Y; Qu L; Pei H; Yildirimer L; Wu Z; Zhang W, DrugDiscov Today 2017, 22 (9), 1302–1317.
9. Weissleder R; Nahrendorf M; Pittet MJ, Nat Mater 2014, 13 (2), 125–38. [PubMed: 24452356]
10. Witmer-Pack MD; Crowley MT; Inaba K; Steinman RM, J Cell Sci 1993, 105 (Pt 4), 965–73. [PubMed: 7693737]
11. Zhang M; Yang M; Bussy C; Iijima S; Kostarelos K; Yudasaka M, Nanoscale 2015, 7 (7), 2834–40. [PubMed: 25597450]
12. Wynn TA; Ramalingam TR, Nat Med 2012, 18 (7), 1028–40. [PubMed: 22772564]
13. Hayden T, Nat Med 2011, 17 (1), 18–20. [PubMed: 21217664]
14. Wynn TA, J Pathol 2008, 214 (2), 199–210. [PubMed: 18161745]
15. Gines P; Graupera I; Lammert F; Angeli P; Caballeria L; Krag A; Guha IN; Murad SD; Castera L, Lancet Gastroenterol Hepatol 2016, 1 (3), 256–260. [PubMed: 28404098]
16. Reichenbach V; Fernandez-Varo G; Casals G; Oro D; Ros J; Melgar-Lesmes P; Weiskirchen R; Morales-Ruiz M; Jimenez W, J Hepatol 2012, 57 (5), 967–73. [PubMed: 22820479]
17. Reichenbach V; Ros J; Fernandez-Varo G; Casals G; Melgar-Lesmes P; Campos T; Makriyannis A; Morales-Ruiz M; Jimenez W, J Pharmacol Exp Ther 2012, 340 (3), 629–37. [PubMed: 22160265]
18. Munoz-Luque J; Ros J; Fernandez-Varo G; Tugues S; Morales-Ruiz M; Alvarez CE; Friedman SL; Arroyo V; Jimenez W, J Pharmacol Exp Ther 2008, 324 (2), 475–83. [PubMed: 18029545]
19. Oro D; Yudina T; Fernandez-Varo G; Casals E; Reichenbach V; Casals G; Gonzalez de la Presa B; Sandalinas S; Carvajal S; Puntes V; Jimenez W, J Hepatol 2016, 64 (3), 691–8. [PubMed: 26519601]
20. Higashi T; Friedman SL; Hoshida Y, Adv DrugDeliv Rev 2017, 121, 27–42.
21. Tsuchida T; Friedman SL, Nat Rev Gastroenterol Hepatol 2017, 14 (7), 397–411. [PubMed: 28487545]
22. Forbes SJ; Rosenthal N, Nat Med 2014, 20 (8), 857–69. [PubMed: 25100531]
23. Melgar-Lesmes P; Edelman ER, J Hepatol 2015, 63 (4), 917–25. [PubMed: 26022689]
24. Tacke F, J Hepatol 2017, 66 (6), 1300–1312. [PubMed: 28267621]
25. Duarte S; Baber J; Fujii T; Coito AJ, Matrix Biol 2015, 44–46, 147–56.
26. Arpino V; Brock M; Gill SE, Matrix Biol 2015, 44–46, 247–54.
27. Murphy FR; Issa R; Zhou X; Ratnarajah S; Nagase H; Arthur MJ; Benyon C; Iredale JP, J Biol Chem 2002, 277 (13), 11069–76. [PubMed: 11796725]
28. Muftuoglu TM; Koksal N; Ozkutlu D, J Am Coll Surg 2000, 191 (6), 668–71. [PubMed: 11129817]
29. Anghelina M; Krishnan P; Moldovan L; Moldovan NI, Am J Pathol 2006, 168 (2), 529–41. [PubMed: 16436667]

30. Jain K; Kesharwani P; Gupta U; Jain NK, Int JPharm 2010, 394 (1–2), 122–42. [PubMed: 20433913]
31. Duncan R; Izzo L, Adv Drug Deliv Rev 2005, 57 (15), 2215–37. [PubMed: 16297497]
32. Gustafson HH; Holt-Casper D; Grainger DW; Ghandehari H, Nano Today 2015, 10 (4), 487–510. [PubMed: 26640510]
33. Li J; Liang H; Liu J; Wang Z,. Int J Pharm 2018, 546 (1–2), 215–225. [PubMed: 29787895]
34. Santos JL; Pandita D; Rodrigues J; Pego AP; Granja PL; Balian G; Tomas H, Mol Pharm 2010, 7 (3), 763–74. [PubMed: 20230026]
35. Perez-Martinez FC; Carrion B; Lucio MI; Rubio N; Herrero MA; Vazquez E; Cena V, Biomaterials 2012, 33 (32), 8152–9. [PubMed: 22858003]
36. Zajac E; Schweighofer B; Kupriyanova TA; Juncker-Jensen A; Minder P; Quigley JP; Deryugina EI, Blood 2013, 122 (25), 4054–67. [PubMed: 24174628]
37. Wang N; Liang H; Zen K, Front Immunol 2014, 5, 614. [PubMed: 25506346]
38. Das A; Sinha M; Datta S; Abas M; Chaffee S; Sen CK; Roy S, Am J Pathol 2015, 185 (10), 2596–606. [PubMed: 26118749]
39. Roderfeld M; Weiskirchen R; Wagner S; Berres ML; Henkel C; Grotzinger J; Gressner AM; Matern S; Roeb E, FASEB J 2006, 20 (3), 444–54. [PubMed: 16507762]
40. Baldassarre M; Pompeo A; Beznoussenko G; Castaldi C; Cortellino S; McNiven MA; Luini A; Buccione R, Mol Biol Cell 2003, 14 (3), 1074–84. [PubMed: 12631724]

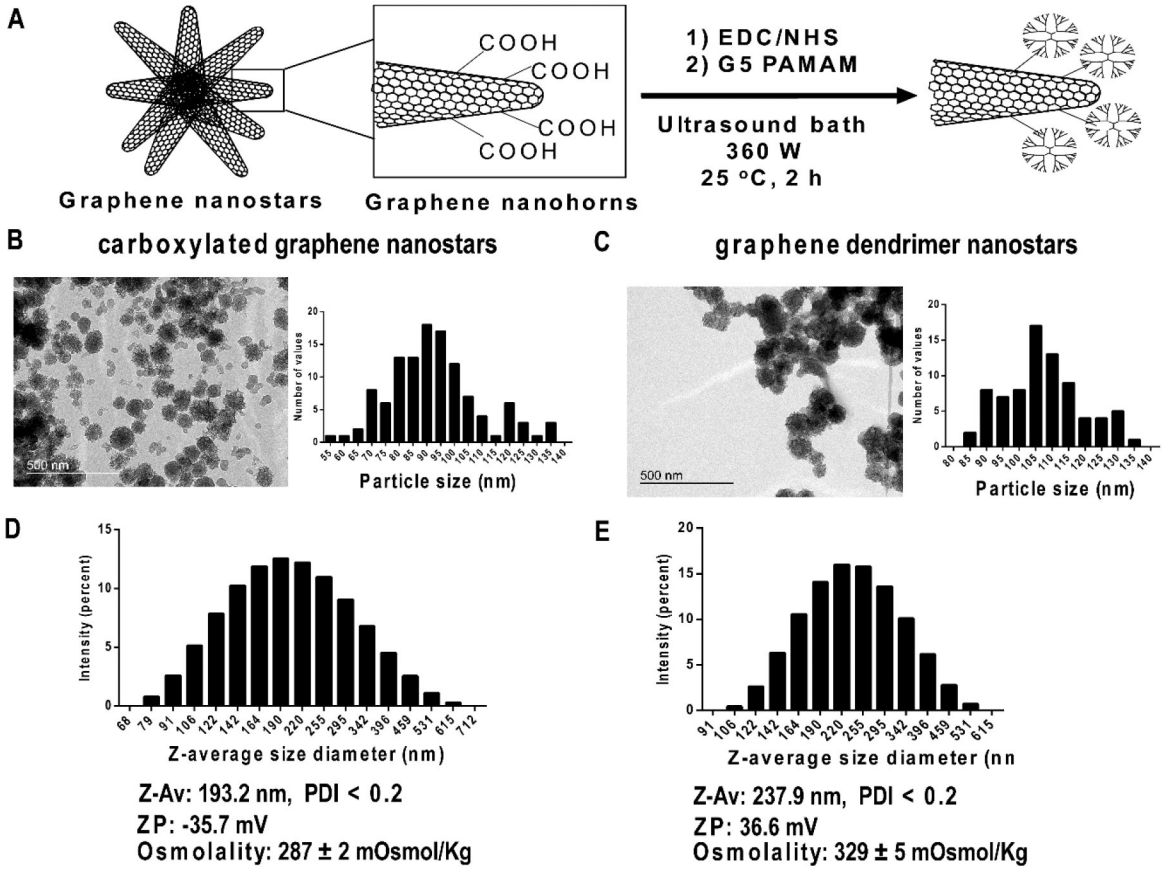


**Figure 1. Synthesis and physicochemical characterization of dendrimer graphene nanostars**

(A) Schematic representation of carboxylated graphene nanostars functionalization method. (B) Representative image of carboxylated graphene nanostars by Transmission Electron Microscopy (TEM) and the corresponding particle size histogram. (C) Representative TEM image of graphene dendrimer nanostars and the corresponding particle size histogram. (D) Particle hydrodynamic size histogram of carboxylated graphene nanostars obtained with Dynamic light scattering (DLS) showing the values of z-average (ZAv), zeta potential (ZP), and formulation osmolality measured with an osmometer. (E) Particle hydrodynamic size histogram of graphene dendrimer nanostars obtained with Dynamic light scattering (DLS) showing the values of z-average (Z-Av), zeta potential (ZP), and formulation osmolality. Polydispersity index (PDI) was lower than 0.2 in all compositions. Osmolality values are mean ± S.E.M. TEM magnification: 120,000x.

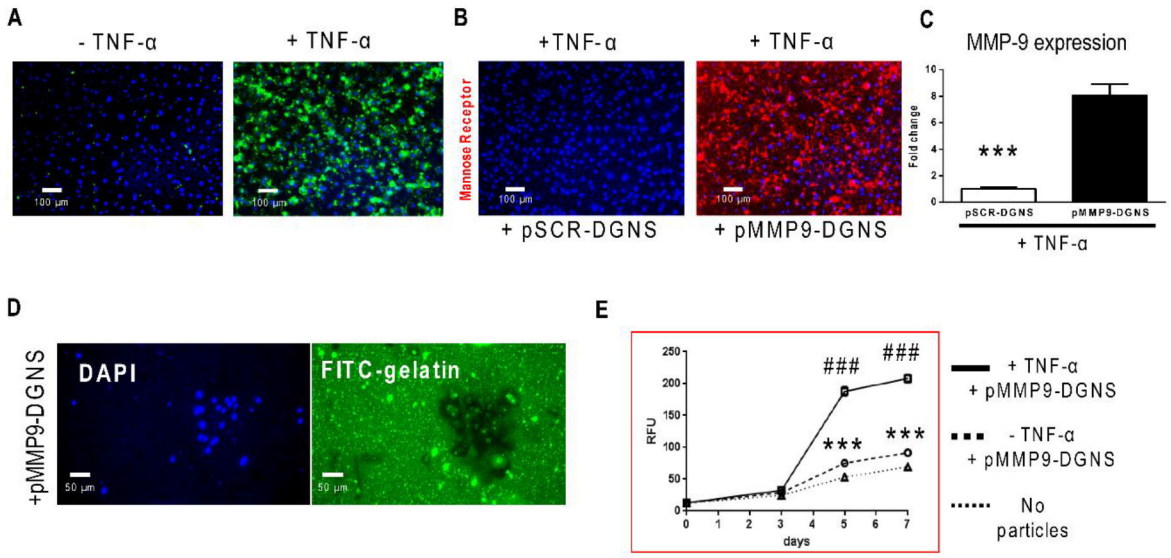


**Figure 2. Functional assay of plasmid transfection efficiency and M2-subset formation using plasmid-dendrimer graphene nanostars.**

(A) Representative fluorescence microscope images of RAW 264.7 macrophages incubated with plasmid expressing MMP-9 (under the control of a CD11b promoter) linked to dendrimer graphene nanostars (pMMP9-DGNS) in the presence or absence of TNF-α (5 ng/mL) for 3 days. Functional constitutive expression of plasmid-derived enhanced green fluorescent protein (eGFP) is highlighted in green (B) Representative fluorescence microscope images of RAW 264.7 macrophages incubated with either a scramble (pSCR) or pMMP9-DGNS in the presence of TNF-α (5 ng/mL) for 3 days and stained for the M2 macrophage marker mannose receptor (in red). (C) Quantification of MMP-9 gene expression by Real-time PCR in RAW 264.7 macrophages inflamed with TNF-α (5 ng/mL) and treated with pSCR-DGNS or pMMP9-DGNS. (D) Representative fluorescence microscope images of RAW 264.7 macrophages seeded onto FITC-gelatin coated plates and incubated with pMMP9-DGNS for 5 days. DAPI stained nuclei (in blue). (E) Quantitative analysis of FITC-gelatin degradation measuring FITC-gelatin released over time to the cell culture medium from macrophages incubated with pMMP9-DGNS in the presence or absence of TNF-α (5 ng/mL) for 7 days using Fluorescence Spectrophotometry. Values are mean ± S.E.M. *** indicates $P \leq 0.0001$ using a Student's t-test vs. no particles; ### indicates $P \leq 0.0001$ using a Student's t-test vs. pMMP9-DGNS without TNF-α.

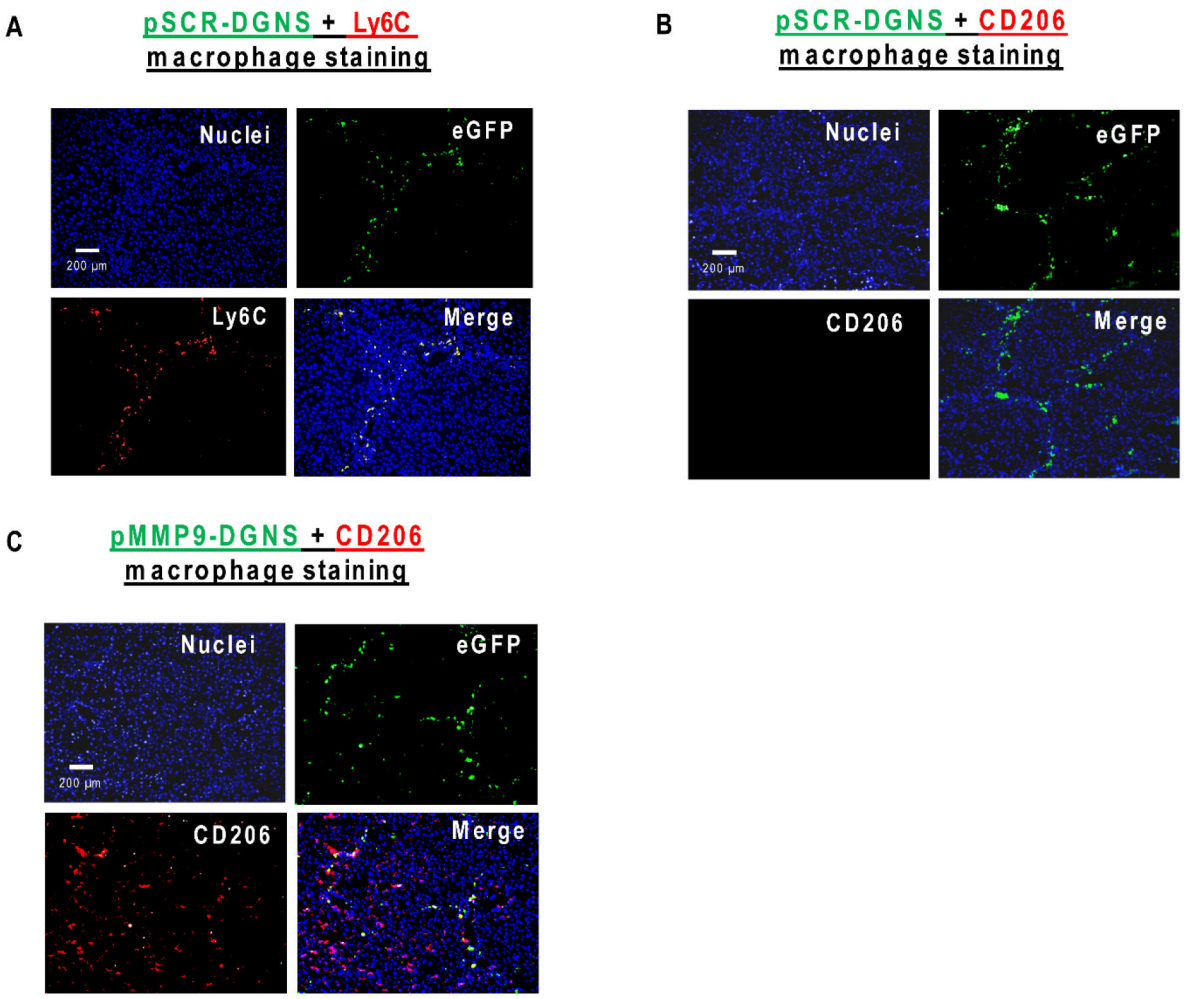


**Figure 3.** ***In vivo*** **efficient gene therapy of pDNA-DGNS targeted to macrophages infiltrated in hepatic fibrotic tracts from cirrhotic mice.**

(A) Representative images of immunofluorescent staining for Ly6C (M1 inflammatory macrophages in red) and detection of functional plasmids (eGFP in green) into macrophages in liver tissue slices from cirrhotic animals treated with scramble plasmid linked to dendrimer graphene nanostars (pSCRDGNS). Cell nuclei were stained with DAPI (in blue). Merge shows cells co-localizing for eGFP and Ly6C. (B) Representative images of immunofluorescent staining for CD206 (mannose receptor in red) and detection of functional plasmids (eGFP in green) into macrophages in liver tissue slices from cirrhotic animals treated with pSCR-DGNS. Cell nuclei were stained with DAPI (in blue). Merge indicates the overlapping between the image corresponding to cells expressing eGFP and the image of the CD206 staining. (C) Representative images of immunofluorescent staining for CD206 (mannose receptor in red) and detection of functional plasmids (eGFP in green) into macrophages in liver tissue slices from cirrhotic animals treated with MMP-9 plasmid linked to dendrimer graphene nanostars (pMMP9-DGNS). Cell nuclei were stained with DAPI (in blue). Merge shows cells co-localizing for eGFP and CD206.

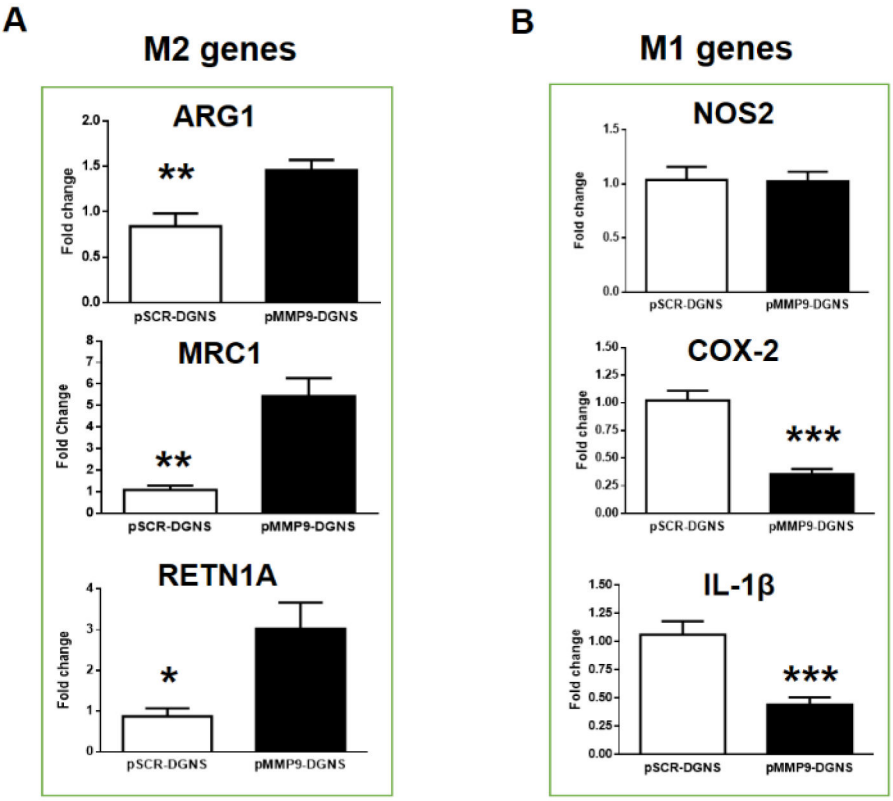


**Figure 4. Hepatic immunomodulation of macrophages gene expression profiles in cirrhotic mice treated with pMMP9-DGNS.**

(A) Quantification of gene expression profiles of M2 macrophages (Arg1, MRC1 and Retn1a) in cirrhotic livers from mice treated with scramble plasmid linked to dendrimer graphene nanostars (pSCR-DGNS) or MMP-9 plasmid linked to dendrimer graphene nanostars (pMMP9-DGNS) by Real-time PCR. (B) Quantification of gene expression profiles of M1 macrophages (iNOS, COX-2 and IL1-β) in cirrhotic livers from mice treated with pSCR-DGNS or pMMP9-DGNS by Real-time PCR. *** indicates $P \leq 0.0001$, ** indicates $P \leq 0.01$, * indicates $P \leq 0.05$ using a Student's t-test. Values are mean ± S.E.M.

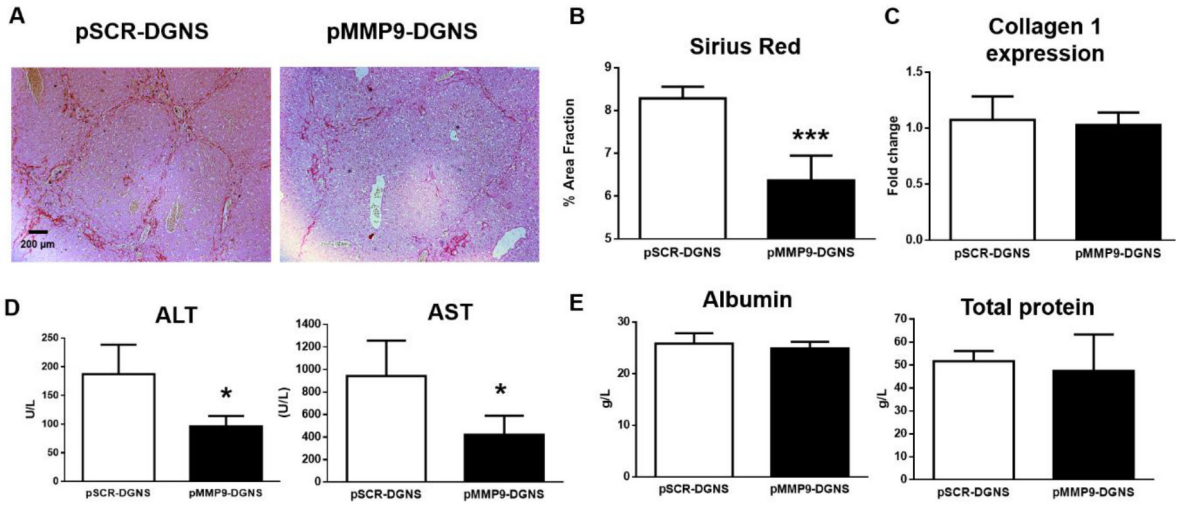


**Figure 5. Effect of macrophage-targeted pMMP9-DGNS gene therapy on liver fibrosis and hepatic function.**

(A) Representative images of Sirius red staining in liver sections from cirrhotic mice treated either with scramble plasmid linked to dendrimer graphene nanostars (pSCR-DGNS) or with MMP-9 plasmid linked to dendrimer graphene nanostars (pMMP9-DGNS). (B) Relative fibrosis area quantified with ImageJ in Sirius Red-stained liver sections from cirrhotic mice treated with either pSCR-DGNS or pMMP9-DGNS. (C) Quantification of Collagen I gene expression by Real-time PCR in liver from cirrhotic mice treated with either pSCR-DGNS or pMMP9-DGNS. (D) Serum markers of liver damage alanine aminotransferase (ALT) and aspartate aminotransferase (AST) quantified in cirrhotic animals treated with either pSCR-DGNS or pMMP9-DGNS. (E) Serum albumin and total proteins quantified in cirrhotic animals treated with either pSCR-DGNS or pMMP9-DGNS. *** indicates $P \leq 0.0001$, * indicates $P \leq 0.05$ using a Student's t-test. Values are mean ± S.E.M.